

Article

A Study on Greenhouse Gas (PFCs) Reduction in Plasma Scrubbers to Realize Carbon Neutrality of Semiconductors and Displays

Bong Jae Lee ^{1,*}, Yujin Hwang ¹, Dong Ki Jo ¹ and Jongmoon Jeong ²

¹ Korea Testing & Research Institute (KTR), 98 Gyoyukwon-ro, Gwacheon-si 13810, Gyeonggi-do, Republic of Korea; wls0348@ktr.or.kr (Y.H.); ehdlr05@ktr.or.kr (D.K.J.)

² GnBS eco, 401-14 Mosan-ro, Daedeok-myeon, Anseong-si 17541, Gyeonggi-do, Republic of Korea; jmjeong@gnbseng.com

* Correspondence: jae8076@ktr.or.kr; Tel.: +82-2-2092-4056

Abstract: Perfluorinated compounds (PFCs) are used for manufacturing purposes in the semiconductor and display industries, resulting in an increased need for emission reduction due to the significant global warming potential of the associated greenhouse gases. The decomposition characteristics of etch-type and water film (WF)-type plasma-wet scrubbers were investigated. The PFCs used in the study were CF₄, SF₆, NF₃, CHF₃, C₂F₆, C₃F₈, and C₄F₈, and the destruction removal efficiency (DRE) and by-product gas generation rate were confirmed based on the changes in the parameters (total flow rate and power) of the plasma-wet scrubber. When the total flow rate reached 100 L/min and the measured maximum power (11 kW), the reduction efficiency of CF₄ in the etch type was 95.60% and the DRE of other PFCs was 99.99%. Moreover, for the WF type, the DRE of CF₄ was 90.06%, that of SF₆ was 96.44%, and that of other PFCs was 99.99%. When the total flow rate reached 300 L/min and 11 kW, the DRE of SF₆ in the etch type was 99%, and the DRE of NF₃, CHF₃, C₂F₆, C₃F₈, and C₄F₈ was 95.57%, 87.06%, 70.74%, 81.45%, and 95.59%, respectively. In addition, in the WF type, the DRE of SF₆ was 94.39%, and the DRE of NF₃, CHF₃, C₂F₆, C₃F₈, and C₄F₈ was 99.80%, 95.34%, 85.38%, 88.49%, and 98.22%, respectively. The decomposition efficiency was high for the etch type for gases with small flow rates or no by-product gas generation. The by-product gas generation rate was significantly lower for the WF type.

Keywords: PFCs; plasma-wet scrubber; DRE; by-product



Citation: Lee, B.J.; Hwang, Y.; Jo, D.K.; Jeong, J. A Study on Greenhouse Gas (PFCs) Reduction in Plasma Scrubbers to Realize Carbon Neutrality of Semiconductors and Displays. *Atmosphere* **2023**, *14*, 1220. <https://doi.org/10.3390/atmos14081220>

Academic Editors: Pengfei Li, Liqiang Wang and Jingzhao Lu

Received: 29 June 2023

Revised: 20 July 2023

Accepted: 23 July 2023

Published: 28 July 2023



Copyright: © 2023 by the authors. Licensee MDPI, Basel, Switzerland. This article is an open access article distributed under the terms and conditions of the Creative Commons Attribution (CC BY) license (<https://creativecommons.org/licenses/by/4.0/>).

1. Introduction

Mixed gases of various compositions are used in the semiconductor and display industries, and CO₂, CF₄, SF₆, and N₂O are mainly emitted as waste gases. Perfluorinated compounds (PFCs) such as CF₄, SF₆, CHF₃, and C₃F₈ are widely used in etching, deposition, and cleaning processes in the semiconductor and display industries [1–3]. PFCs have a significant impact on global warming because their global warming potential (GWP) and lifetime are very high compared to that of CO₂ and CH₄. Table 1 shows the latest GWP and lifetime of greenhouse gases provided by the IPCC's sixth assessment report (AR6). PFCs were designated one of the six major greenhouse gases in the 1997 Kyoto Protocol and regulated internationally for their emissions [4,5]. Emissions of PFCs are increasing with the growth of the semiconductor and display industries. As international interest in carbon reduction increases, the reduction of PFCs is necessary [6,7].

To reduce PFC emissions, process optimization, recycling/recovery, and reduction technologies are proposed. None of the existing gases with low GWP are a suitable replacement for PFCs, and it takes a long time to develop alternative gases. In addition, semiconductor and display manufacturing processes are complex, making it difficult to optimize processes for the reduction or implementation of recycling and recov-

ery facilities [8–11]. During the etching and deposition process, PFCs are used in an optimal ratio to improve the product's completeness, making it difficult to change the process conditions [12,13].

Scrubbers used in the semiconductor and display industries were initially developed to remove air pollutants. As interest in greenhouse gas emissions increased, scrubbers were developed and improved to handle greenhouse gases as well [14]. There are various types of scrubbers which vary in terms of treatment efficiency, from higher to lower: these include heat, burn, and plasma, in that order [15]. In order to increase PFC treatment, wet treatment facilities are combined at the rear of the reduction device to be used as burn-wet, plasma-wet, etc. [16]. On industrial sites, burn-wet scrubbers are used most frequently. Research on the plasma-wet type, which has a higher PFC destruction removal efficiency (DRE) than the burn-wet type, is being actively conducted, and its utilization in the field is increasing accordingly. Plasma scrubber research was mainly conducted by improving the plasma torch [17] and the wet processing structure [18]. However, when measurements were taken, the DRE of PFCs was the main focus, and only the type of gas by-product produced by each PFC was confirmed; no study focused on the amount of gas by-product generated.

In this study, the plasma wet scrubber, which is seeing increasing use in the field, was divided into an etch type and a water film (WF) type. In addition, each type of DRE and by-product gas generation rate was measured. The DRE of PFCs was measured using the plasma power and total flow rate as parameters. By adjusting the parameters for each type of PFC, the optimal conditions were confirmed to confirm under which conditions the DRE was high. The by-product gas generation rate of PFCs was measured under a power condition in which the DRE of all PFCs was greater than 99%. By checking the DRE and considering the by-product gas generation rate, the optimal type of plasma-wet scrubber for each type of PFC was confirmed.

Table 1. Global warming potential and lifetime of greenhouse gases (AR6) [19].

Greenhouse Gases	Lifetime (Year)	GWP ₁₀₀
CO ₂	50–200	1
CH ₄	12	27
CF ₄	50,000	7380
SF ₆	3200	24,300
C ₂ F ₆	10,000	12,400
CHF ₃	222	14,600
C ₃ F ₈	2600	9290
C ₄ F ₈	3200	10,200
NF ₃	500	17,400

2. Materials and Methods

2.1. Composition of Plasma-Wet Scrubber

Figure 1 shows the configuration of the plasma-wet scrubber. The plasma-wet scrubber is composed of an inlet part, plasma system, pyrolysis reactor, gas quenching part, wastewater circulation tank, wet spray tower, and outlet part. When waste gas such as PFCs enters the inlet part, it comes into contact with the arc plasma generated by the plasma system and rises up in the pyrolysis reactor to decompose. The high-temperature gas is cooled in the quenching part and by-products are treated in the wet spray tower. The wastewater is stored in the circulation tank and discharged. The treated gas is discharged through the outlet [20]. In this paper, the type of plasma used at the plasma-wet scrubber was high-temperature arc plasma, and nitrogen was used as the discharge gas. When plasma is generated in a plasma system, the temperature at the center and at the edge represents several tens of thousands to thousands of degrees. The detailed specifications of the plasma-wet scrubber are provided in Table 2.

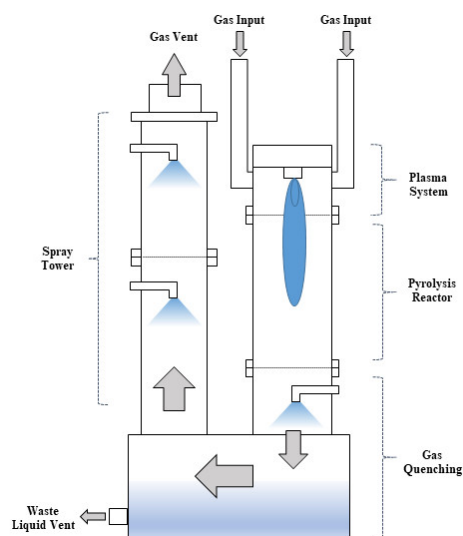


Figure 1. Schematic diagram of plasma-wet scrubber.

Table 2. Specification of plasma-wet scrubber.

Contents	Plasma-Wet Scrubber
Type of plasma	Arc
Maximum plasma power	15 kW
Frequency of plasma	60 Hz
Voltage of plasma	208 VAC
Phase	3 phase
Dimension (W × D × H)	800 × 800 × 1836

Figure 2 shows the setup of the plasma-wet scrubber used in this study. The plasma-wet scrubber is divided into an etch type for waste gas treatment during the etching process and a water film type for waste gas treatment during the chemical vapor deposition process. For the etch type, water is sprayed from the gas quenching part located below the pyrolysis reactor part. For the water film type, a water film is formed inside the pyrolysis reactor part.

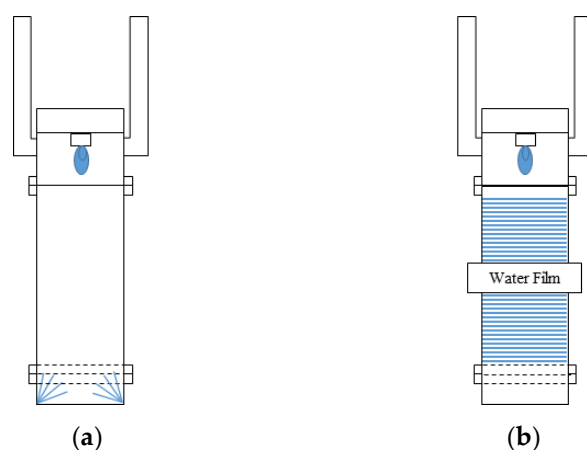


Figure 2. Schematic diagram of (a) etch type and (b) water film type.

2.2. Experiment Setup and Methods

Figure 3 illustrates the experiment setup that was used in this study. CF_4 , SF_6 , NF_3 , CHF_3 , C_2F_6 , C_3F_8 , and C_4F_8 were used, each with high purity (99.999%). The flow rate of the target gas was adjusted using a mass flow meter (M3030V, LINE TECH Co., Daejeon, Republic of Korea), and the concentration of the PFC gas was adjusted to 4000 to 5000 $\mu\text{mol/mol}$ via mixing with nitrogen gas (99.999%) prior to injection into the plasma-wet scrubber

(NSPW600Plus, GnBS eco, Anseong, Republic of Korea). The flow rate injected into the plasma-wet scrubber was between 100 and 300 L/min; this included nitrogen and air, which are essential during scrubber operation. Plasma-wet scrubbers range in power from 6 to 11 kW. Fourier transform infrared spectroscopy (FT-IR; Gasetmet DX4000, Gasetmet Co., Vantaa, Finland) was used to measure the inlet and outlet concentrations of the Plasma-wet scrubber. For the gas cell of FT-IR, a 60 cm-long cell was used in the inlet measurement, and a 500 cm-long cell was used in the outlet measurement. The inlet and outlet flow rates of the plasma-wet scrubber were measured using a quadrupole mass spectrometer (isepa-S, el Co., Daejeon, Republic of Korea). Table 3 shows the experimental operating conditions in detail.

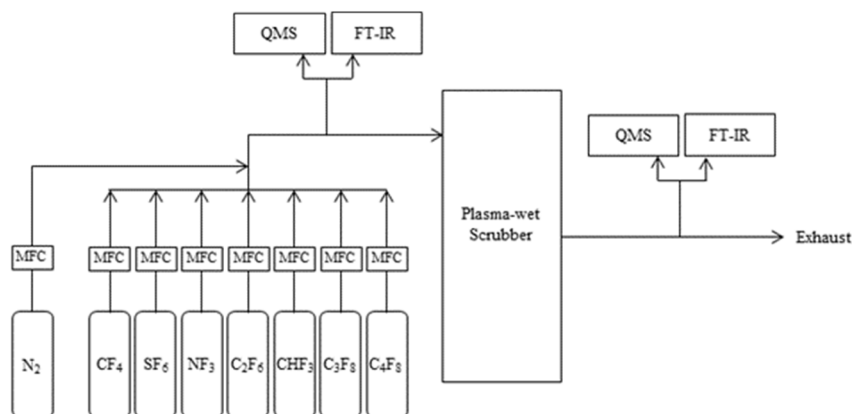


Figure 3. Schematic diagram of experiment.

Table 3. Operating conditions of experiment.

Operating Condition	Parameter
Input power (kW)	6–11
Total gas flow rate (L/min)	100, 300
N ₂ plasma gas flow rate (L/min)	40~50
Reactive injection gas(air) flow rate(L/min)	0.8~2
Concentration of PFCs (μmol/mol)	4000–5000

2.3. Calculation of PFCs

The DRE of PFCs can be defined as follows [21]:

$$\text{DRE of PFCs (\%)} = \left(1 - \frac{V_{out}}{V_{in}}\right) \times 100 \tag{1}$$

$$V_{in} = C_{in} \times Q_{in} \tag{2}$$

$$V_{out} = C_{out} \times Q_{out} \tag{3}$$

where V_{in} : inlet volume-flow of PFCs (L/min); V_{out} : outlet volume flow of PFCs (L/min); C_{in} : inlet concentration of PFCs (μmol/mol); C_{out} : outlet concentration of PFCs (μmol/mol); Q_{in} : inlet flow of PFCs (L/min); Q_{out} : outlet flow of PFCs (L/min).

The generation rate of by-products can be defined as follows:

$$\text{Generation rate of By – products (\%)} = \frac{V_{bp}}{V_{in}} \times 100 \tag{4}$$

$$V_{bp} = C_{bp} \times Q_{out} \tag{5}$$

where V_b : outlet volume-flow of by-products (L/min); C_{bp} : outlet concentration of by-products (μmol/mol).

2.4. Mechanism of Reactions

Table 4 shows the mechanism of PFCs using plasma. PFCs are dissociated and ionized into CF_x (CF_3 , CF_2 , CF), C_xF_x (C_3F_7 , C_3F_5 , C_2F_4 , etc.), CHF_x (CHF_2 , CHF), SF_x (SF_5 , SF_4 , SF_3), and NF_x (NF_2 , NF) through collisions with electrons (e) according to Equations (6)–(48). As shown in Equations (49)–(60), recombination achieved via secondary reactions between gases was considered. The water sprayed down the pyrolysis reactor in the etch type and the WF in the WF type generated OH and H radicals through electrons (e) according to Equation (61). The generated OH and H radicals were converted to HF via a reaction with the decomposed PFCs, according to Equations (62)–(70) [22–35].

Table 4. The reaction of dissociation and formation for PFCs.

Reaction	Number
Dissociation and Ionization	
$C_4F_8 + e \rightarrow C_3F_5^+ + CF_2 + F + 2e$	(6)
$C_4F_8 + e \rightarrow C_2F_4^+ + C_2F_4 + 2e$	(7)
$C_4F_8 + e \rightarrow C_4F_7 + F^-$	(8)
$C_4F_8 + e \rightarrow 2C_2F_4 + e$	(9)
$C_3F_8 + e \rightarrow C_3F_7^+ + F$	(10)
$C_3F_8 + e \rightarrow C_2F_5^+ + CF_3$	(11)
$C_3F_8 + e \rightarrow C_2F_4^+ + CF_4$	(12)
$C_3F_8 + e \rightarrow C_2F_4^+ + CF_3 + F$	(13)
$C_4F_7 + e \rightarrow C_2F_4 + C_2F_3 + e$	(14)
$C_2F_3 + e \rightarrow CF_2 + CF + e$	(15)
$C_3F_7 + e \rightarrow C_2F_5 + CF_2 + e$	(16)
$C_3F_7 + e \rightarrow CF_3^+ + C_2F_4 + e$	(17)
$C_2F_5 + e \rightarrow CF_3^+ + CF_2 + e$	(18)
$C_2F_5 + e \rightarrow C_2F_4 + F^- + e$	(19)
$C_2F_4 + e \rightarrow CF_3^+ + CF + e$	(20)
$C_2F_4 + e \rightarrow 2CF_2 + e$	(21)
$C_2F_3 + e \rightarrow CF^+ + CF_2 + e$	(22)
$CHF_3 + e \rightarrow CHF_2 + F + e$	(23)
$CHF_3 + e \rightarrow CF_3 + H + e$	(24)
$CHF_2 + e \rightarrow CHF + F + e$	(25)
$CHF_2 + e \rightarrow CF_2 + H + e$	(26)
$CHF + e \rightarrow CF + H + e$	(27)
$C_2F_6 + e \rightarrow 2CF_3 + e$	(28)
$C_2F_6 + e \rightarrow CF_3^+ + CF_3 + 2e$	(29)
$C_2F_6 + e \rightarrow CF_2^+ + CF_4 + 2e$	(30)
$C_2F_6 + e \rightarrow CF^+ + CF_4 + F + 2e$	(31)
$C_2F_6 + e \rightarrow F^- + CF_2 + CF_3$	(32)
$CF_4 + e \rightarrow CF_3 + F + e$	(33)
$CF_4 + e \rightarrow CF_2 + 2F + e$	(34)
$CF_4 + e \rightarrow CF_3^+ + F + 2e$	(35)
$CF_4 + e \rightarrow CF_3 + F^+ + 2e$	(36)
$CF_3 + e \rightarrow CF_2 + F + e$	(37)
$CF_2 + e \rightarrow CF + F + e$	(38)
$CF_2 + e \rightarrow C + 2F + e$	(39)
$CF + e \rightarrow C + F + e$	(40)
$SF_6 + e \rightarrow SF_5 + F + e$	(41)
$SF_6 + e \rightarrow SF_4 + 2F + e$	(42)
$SF_6 + e \rightarrow SF_3 + 3F + e$	(43)
$SF_5 + e \rightarrow SF_4 + F + e$	(44)
$SF_4 + e \rightarrow SF_3 + F + e$	(45)
$NF_3 + e \rightarrow NF_2 + F + e$	(46)
$NF_3 + e \rightarrow NF + F_2 + e$	(47)
$NF_3 + e \rightarrow NF + F^-$	(48)

Table 4. Cont.

Reaction	Number
Recombination	
$C_3F_8 + CF_3^+ \rightarrow CF_4 + C_3F_7^+$	(49)
$C_3F_8 + C_2F_5^+ \rightarrow C_2F_6 + C_3F_7^+$	(50)
$CHF_3 + F \rightarrow CF_3 + HF$	(51)
$CHF_2 + F \rightarrow CF_2 + HF$	(52)
$CHF_2 + CF_3 \rightarrow CHF_3 + CF_2$	(53)
$CHF + F \rightarrow CF + HF$	(54)
$CF_3 + F + e \rightarrow CF_4 + e$	(55)
$CF_2 + F + e \rightarrow CF_3 + e$	(56)
$CF + F + e \rightarrow CF_2 + e$	(57)
$SF_5 + F \rightarrow SF_6$	(58)
$SF_4 + F \rightarrow SF_5$	(59)
$SF_3 + F \rightarrow SF_4$	(60)
OH and H radical reaction	
$H_2O + e \rightarrow OH + H + e$	(61)
$CF_3 + OH \rightarrow COF_2 + HF$	(62)
$CF_2 + OH \rightarrow COF + HF$	(63)
$CF + OH \rightarrow CO + HF$	(64)
$COF + OH \rightarrow CO_2 + HF$	(65)
$CHF_3 + H \rightarrow CF_3 + H_2$	(66)
$CHF_2 + H \rightarrow CHF + HF$	(67)
$CHF_2 + H \rightarrow CF_2 + H_2$	(68)
$NF_3 + H \rightarrow NF_2 + HF$	(69)
$NF_2 + H \rightarrow NF + HF$	(70)
$SF_5 + OH \rightarrow SOF_4 + HF$	(71)
$SF_4 + OH + F \rightarrow SOF_4 + HF$	(72)
$SF_3 + OH \rightarrow SOF_2 + HF$	(73)

3. Results

3.1. Decomposition of PFCs in Etch Type

Figure 4a shows the DREs of CF_4 , SF_6 , CHF_3 , C_2F_6 , C_3F_8 , and C_4F_8 when the flow rate was 100 L/min in the etch type. The DREs of SF_6 , NF_3 , CHF_3 , C_2F_6 , C_3F_8 , and C_4F_8 were maintained above 99% regardless of power changes. The DRE of CF_4 increased from 72.45% at 8 kW to 95.60% at 11 kW with increasing power, but the DRE was lower compared to other gases. From 6 kW to 11 kW, it can be seen that the high temperature at which the decomposition of SF_6 is optimal was successfully maintained. CF_4 has a stable structure; it difficult to decompose because it requires a high reaction temperature for decomposition, and recombination occurs easily. At the highest power of 11 kW, the high temperature at which the decomposition of CF_4 was successfully maintained.

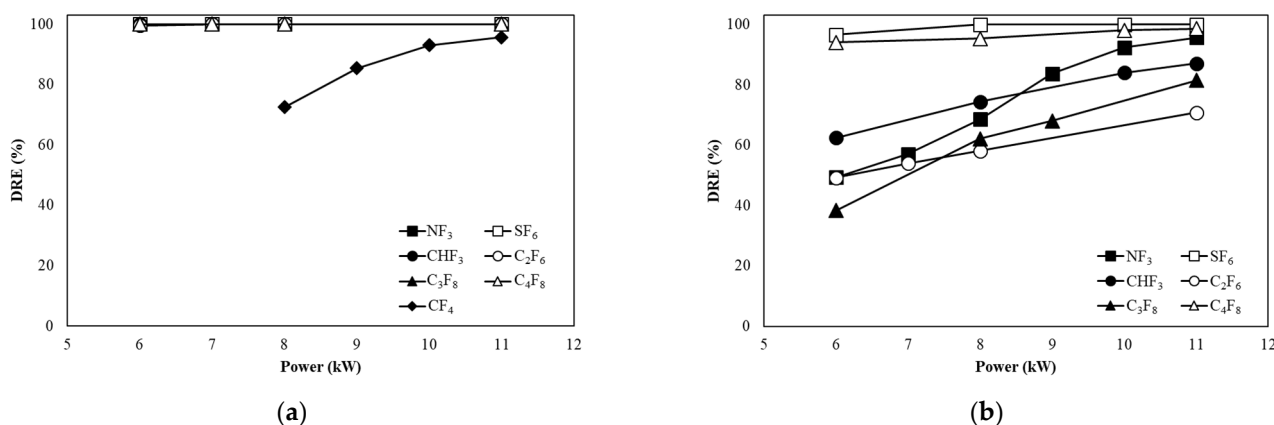


Figure 4. Decomposition of PFCs with power change at a flow rate of (a) 100 L/min and (b) 300 L/min in the etch type.

Figure 4b shows the DREs of SF₆, CHF₃, C₂F₆, C₃F₈, and C₄F₈ when the flow rate was 300 L/min in the etch type. As the power increased, the DRE of SF₆ increased from 96.57% to 99.99%, and the DRE reached 99.99% at 8 kW power, maintaining the DRE up to 11 kW. The DRE of NF₃ increased from 49.32% to 95.57% as the power increased, and from 10 kW, the DRE was over 90%. The DRE of C₄F₈ increased from 94% to 98.59% as the power increased, and from 6 kW, the efficiency was higher than 90%. In the case of CHF₃, C₂F₆, and C₃F₈, as the power increased, the DRE increased from 62.42%, 49.17%, and 38.35% to 87.06%, 70.74%, and 81.45%, respectively. As the flow rate increased, the amount of injected PFCs increased, so that the amount of gas that passed without contacting the plasma increased and does not receive enough energy to decompose. All PFCs showed a lower DRE compared to the flow rate of 100 L/min.

3.2. Decomposition of PFCs in WF Type

Figure 5a shows the DREs of CF₄, SF₆, CHF₃, C₂F₆, C₃F₈, and C₄F₈ when the flow rate is 100 L/min in the water film (WF) type. As the power increased, the DREs of SF₆, CHF₃, C₂F₆, C₃F₈, and C₄F₈ increased from 96.44%, 99.30%, 96.60%, 98.74%, and 99.93% to 99.99%, respectively. For CF₄, the DRE value increased from 43.96% to 90.06% as the power increased from 6 to 11 kW, but the DRE was lower compared to other gases. For NF₃, the DRE was 99.99% at 6 kW regardless of the power increase. For PFCs other than CF₄ and NF₃, the DRE of 6 to 7 kW tended to be lower compared to the DRE of 11 kW. The temperature inside the pyrolysis reactor was slightly reduced due to WF, so the DRE decreased at low power, and as the power increased, the temperature inside the pyrolysis reactor was maintained at a level that did not affect decomposition. CF₄ presented a lower DRE compared to the DRE of other PFCs, although the DRE increased as the power increased. CF₄ requires a high temperature to decompose, but the DRE seems to be low because the WF type cannot maintain a sufficient temperature for CF₄ decomposition.

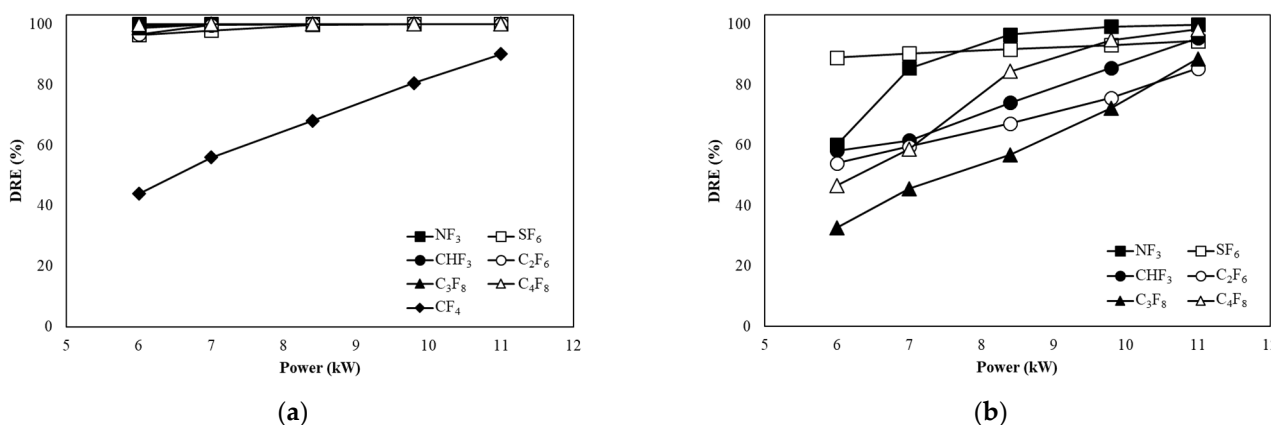


Figure 5. Decomposition of PFCs with power change at a flow rate of (a) 100 L/min and (b) 300 L/min in the WF type.

Figure 5b shows the DREs of SF₆, CHF₃, C₂F₆, C₃F₈, and C₄F₈ when the flow rate was 300 L/min in the WF type. For SF₆, it increased from 88.91% to 94.39% as the power increased. Meanwhile, for NF₃, CHF₃, C₂F₆, C₃F₈, and C₄F₈, the DRE at 6 kW was as low as 60.21%, 58.21%, 54.08%, 32.67%, and 46.60%. However, the DREs of NF₃, CHF₃, C₂F₆, C₃F₈, and C₄F₈ at 11 kW were 99.80%, 95.34%, 85.38%, 88.49%, and 98.22%, respectively. The DRE of SF₆ was 94.39% at maximum power, showing low efficiency compared to the flow rate of 100 L/min. As the flow rate increased, the decomposition became insufficient. Other PFCs also showed low efficiency at 6 kW with DRE compared to a flow rate of 100 L/min, but at the highest power of 11 kW, DRE mostly showed small differences compared with a flow rate of 100 L/min. WF appeared to cause reactions such as those described by Equations (61)–(70) to convert PFCs to HF, increasing the DRE before the decomposed gas recombined into PFCs.

3.3. DRE of Etch and WF Type

Figure 6 shows the DRE of CF_4 in the etch type and WF type when the flow rate was 100 L/min. The etch type maintained a high temperature up to the pyrolysis reactor, so the DRE of CF_4 was greater than that of the WF type. Since CF_4 has a stable C–F binding energy of 543 kJ/mol, the reaction must occur at a very high temperature to achieve decomposition [36]. It can be seen that as the power increased, the plasma size also increased, and CF_4 easily reached a high temperature at which it was easily decomposed, so the C–F bond of CF_4 was well decomposed. Meanwhile, for the WF type, the temperature inside the reactor was lower than that of the etch type due to the water film, so the decomposition of CF_4 was insufficient. As shown by Equations (33)–(36), in order for CF_4 to react with OH and H radicals, decomposition to CF_x must first occur. However, there was less conversion to HF for the WF type compared to the etch type because the decomposition of CF_4 was unsatisfactory.

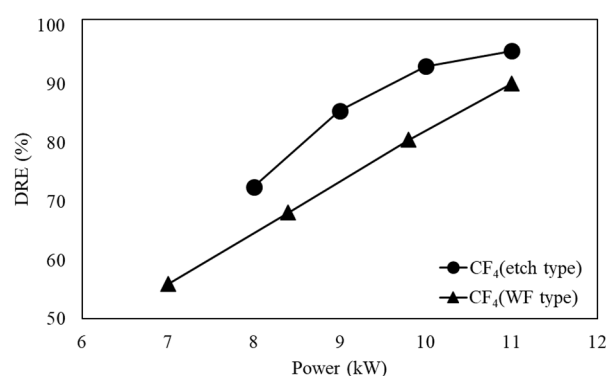


Figure 6. Decomposition of CF_4 in etch type and WF type.

Figure 7 shows the DRE of SF_6 , NF_3 , CHF_3 , C_2F_6 , C_3F_8 , and C_4F_8 in the etch type and WF type when the flow rate is 300 L/min and the power is 11 kW. For SF_6 , the DRE of the etch type was higher than that of the WF type. The S–F binding energy of SF_6 is 438–447 kJ/mol, and the reaction must occur at a high temperature to achieve decomposition [37]. Regardless of the type, the DRE was high at 90% or more, which means that recombination such as that shown by Equations (58)–(60) was insufficient when decomposition occurred as described by Equations (41)–(45). In the WF type, due to the water film, the temperature inside the reactor was lower than that of the etch type, which inhibited the decomposition of SF_6 . In the cases of NF_3 , CHF_3 , C_2F_6 , and C_3F_8 , DRE was higher in the WF type than in the etch type. The N–F bond energy of NF_3 is 278 kJ/mol, so it does not require very high temperatures for decomposition [38]. WF prevented the recombination of each gas by causing a reaction as shown in Equations (62)–(70) and was subsequently converted to HF. For C_4F_8 , the DREs of the etch type and the WF type were similar. As shown in Equations (6)–(9) and (14)–(22), C_4F_8 exhibited a high DRE regardless of the etch type and WF type because the C–F bond was broken in various ways. C_4F_8 is unable to select a type that can be easily decomposed by DRE alone. The optimal type should be selected in consideration of the generation rate of by-product gas generated when C_4F_8 is decomposed.

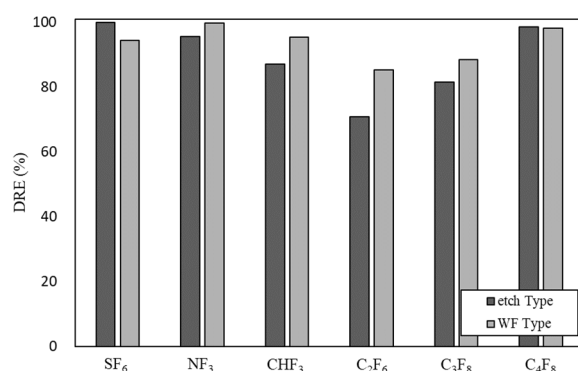


Figure 7. Decomposition of PFCs in etch type and WF type.

3.4. Rate of By-Product Gas Generation

The rate of by-product gas generation was calculated based on the amount of by-product gas generation for C₂F₆, CHF₃, C₃F₈, and C₄F₈, where F gases such as CF₄ and C₂F₆ were generated as by-product gases. The amount of by-product gas generation was measured at a flow rate of 100 L/min and 7 kW power. Figure 8a shows the by-product gas generation rate of CHF₃ in the etch type. The pure DRE was calculated based on a by-product gas generation rate was 89.54%, and the by-product gas generation rate was confirmed to be 10.40%. As for by-product gas, CF₄ was high at 10.37% of the by-product gas generation rate, and C₂F₆ was generated at as little as 0.03%. Figure 8b shows the by-product gas generation rate of CHF₃ for the WF type. The pure DRE calculated based on a by-product gas generation rate was 99.93% and the by-product gas generation rate was 0.002%, showing a very low generation rate. A small amount of CF₄ was generated as a by-product gas. It has been determined that for the etch type, CHF₃ undergoes a recombination reaction similar to that described in Equations (51)–(57), and some recombination occurs as a by-product gas, CF₄. Meanwhile, for the WF type, CHF₃ occurs before the reaction described in Equations (61)–(68) is recombined, and only a small amount of by-product gas (CF₄) is generated, and most of it is converted to HF and treated.

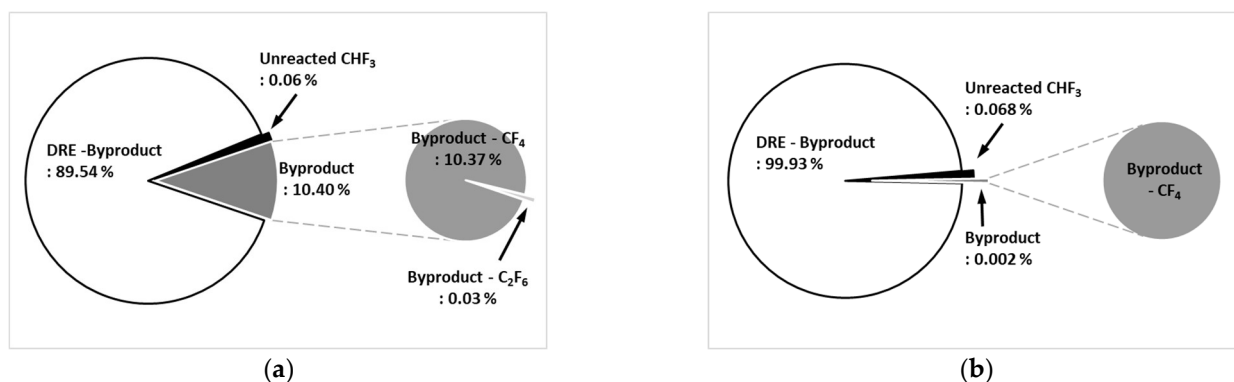


Figure 8. By-product generation rate of CHF₃ for (a) etch type and (b) WF type.

Figure 9a shows the by-product gas generation rate of C₂F₆ in the etch type. The pure DRE was calculated based on a by-product gas generation rate was 65.21%, and the by-product gas generation rate was confirmed to be 34.76%. Only CF₄ was generated as a by-product gas. Figure 9b shows the by-product gas generation rate of C₂F₆ in WF type. It was confirmed that the pure DRE based on the by-product gas generation rate was 99.62% and the by-product gas generation rate was 0.06%, showing a very low generation rate. A small amount of CF₄ was generated as a by-product gas, even for the WF type. For the etch type, some of the recombination reactions of C₂F₆ to CF₄, as shown in Equation (55), occurred. For the WF type, the reaction shown in Equations (61)–(65) occurred before the

recombination reaction; only a small amount of by-product gas (CF_4) was generated, and most of it is converted to HF and treated.

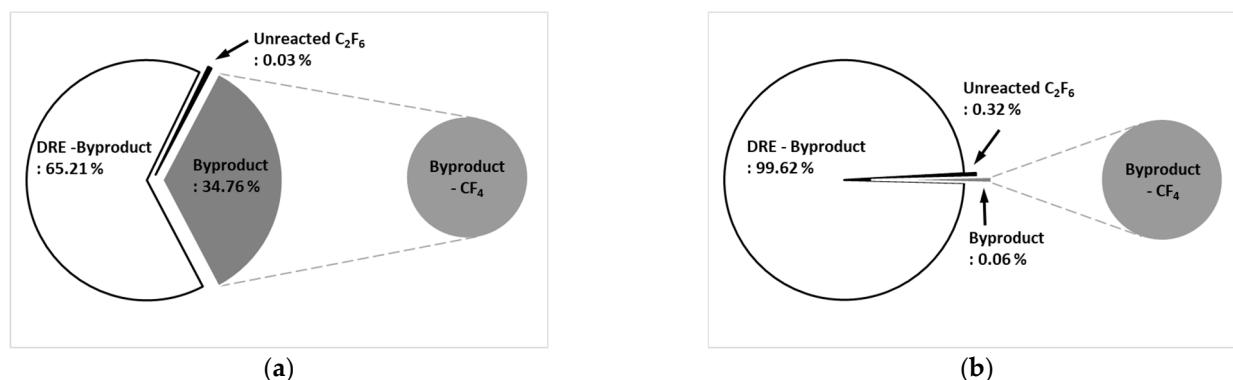


Figure 9. By-product generation rate of C_2F_6 for (a) etch type and (b) WF type.

Figure 10a shows the by-product gas generation rate of C_3F_8 for the etch type. The by-product gas generation rate of C_3F_8 was 130.58%, and more by-product gas was generated than the amount of injected C_3F_8 . As for by-product gas, CF_4 was high at 130.511%, C_2F_6 was 0.068%, and CHF_3 was low at 0.001%. Figure 10b shows the by-product gas generation rate of C_3F_8 for the WF type. The by-product gas generation rate of C_3F_8 was 0.09%, and the pure DRE calculated based on the by-product gas generation rate was confirmed to be 99.76%. For the WF type, a small amount of CF_4 was generated as a by-product of C_3F_8 . Meanwhile, for the etch type, C_3F_8 mainly underwent a recombination reaction as shown in Equations (49)–(57), and all C_3F_8 was not removed but converted to other CF_x and C_xF_x and mainly reacted as shown in Equations (49) and (55) to convert to CF_4 . For the WF type, before the main recombination reaction occurred, the reaction shown in Equations (61)–(65) took place; only a small amount of by-product gas (CF_4) was generated, and most of it was converted to HF and subsequently treated.



Figure 10. By-product generation rate of C_3F_8 for (a) etch type and (b) WF type.

Figure 11a shows the by-product gas generation rate of C_4F_8 for the etch type. The by-product gas generation rate of C_4F_8 was 146.95%, and more by-product gas was generated than the amount of injected C_4F_8 . Among the by-product gases, CF_4 was high at 140.90% and C_2F_6 was low at 0.05%. Figure 11b shows the by-product gas generation rate of C_4F_8 for the WF type. The by-product gas generation rate of C_4F_8 was 20.19%, which was less than that of the etch type, and the pure DRE calculated based on the by-product gas generation rate was confirmed to be 79.80%. For the WF type, as a by-product gas of C_4F_8 , CF_4 was generated at 99.99% and C_2F_6 at 0.01%. Meanwhile, for the etch type, C_4F_8 was converted into CF_x and C_xF_x , mainly as a result of recombination reactions similar to those of C_3F_8 . Evidently, for the WF type, reactions such as Equations (61)–(65) occur more frequently than recombination reactions. Some by-product gases (CF_4 , C_2F_6) are generated, and the rest are

converted to HF and subsequently treated. When calculating greenhouse gas emissions, both DRE and the amount of by-product gas should be taken into consideration. Therefore, when selecting a plasma scrubber according to the type of PFCs, it is necessary to consider a low by-product gas generation rate by checking the final amount of PFCs discharged rather than considering the DRE alone.

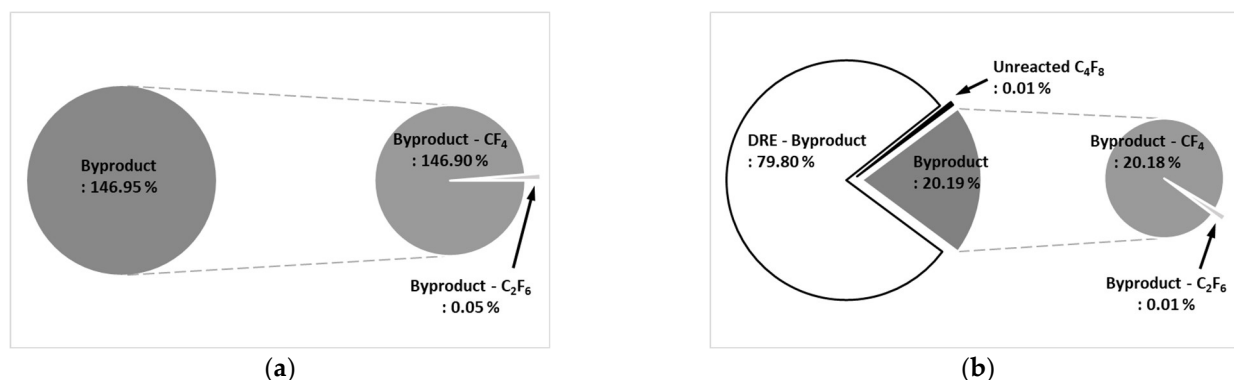


Figure 11. By-product generation rate of C_4F_8 for (a) etch type and (b) WF type.

4. Conclusions

In this study, to evaluate the decomposition characteristics of each type of plasma-wet scrubber, an experiment was conducted to determine the DRE and by-product gas generation rate according to the parameter change of the etch-type and WF-type plasma-wet scrubbers. At 100 L/min and 11 kW in the etch type, the DRE of CF_4 was 95.60%, and the other gases maintained DRE at 99.99% from 6 to 11 kW. At 300 L/min and 11 kW, the reduction efficiencies of SF_6 , NF_3 , CHF_3 , C_2F_6 , C_3F_8 , and C_4F_8 were 99.99%, 95.57%, 87.06%, 70.74%, 81.45%, and 98.59%, respectively. At 100 L/min and 11 kW in the WF type, the DRE of CF_4 was 90.06% and the DRE of SF_6 was 96.44%, and most of the other gases showed a DRE of 99.99%. In addition, at 300 L/min and 11 kW, the DREs of SF_6 , NF_3 , CHF_3 , C_2F_6 , C_3F_8 , and C_4F_8 were 94.39%, 99.80%, 95.34%, 85.38%, 88.49%, and 98.22%, respectively. The DRE of CF_4 and SF_6 in the etch type was smaller than that of the WF type. It appears that the temperature inside the reactor was lower than that of the etch type, so decomposition did not occur properly and the DRE was lowered. In addition, the DRE of WF was high at a total gas flow rate of 300 L/min. This indicates that recombination was prevented by the water film and that the DRE was increased. Therefore, in the process using CF_4 and SF_6 , the etch type was considered, and in the process using other gases, the WF type was considered.

It was confirmed that the by-product gas generation rate showed a significant decrease for the WF type compared to the etch type. This seems to have reduced the generation of by-product gases by applying HF conversion prior to their decomposition into by-product gases such as CF_4 and C_2F_6 due to the treatment of water film and by-products. Therefore, the use of a WF-type plasma-wet scrubber can be considered while using CHF_3 , C_2F_6 , C_3F_8 , and C_4F_8 , which generate by-product gases. However, for CF_4 or SF_6 , which require high temperatures to achieve decomposition, an etch-type plasma-wet scrubber is considered rather than the WF type. The results of this study are expected to assist with the selection of the optimal plasma-wet scrubber according to the PFCs used in order to realize carbon neutrality in the semiconductor and display industries.

Author Contributions: All authors contributed to the research presented in this work. Their contributions are as follows. Conceptualization, Y.H.; investigation, D.K.J. and J.J.; writing—original draft preparation, B.J.L. All authors have read and agreed to the published version of the manuscript.

Funding: This work was supported by the Korea Evaluation Institute of Industrial Technology (KEIT) through the “Next-generation Intelligent Semiconductor Technology Development Project”, funded by the Korean Ministry of Trade, Industry and Energy (MOTIE). (No.20016238) and the Korea

Environment Industry & Technology Institute (KEITI) through the “Climate Change R&D Project for New Climate Regime”, funded by the Korean Ministry of Environment (MOE) (No.2022003560008).

Institutional Review Board Statement: Not applicable.

Informed Consent Statement: Not applicable.

Data Availability Statement: Not applicable.

Conflicts of Interest: The authors declare no conflict of interest.

Abbreviations

PFCs	Perfluorinated compounds.
GWP	Global warming potential.
DRE	Destruction removal efficiency.
FT-IR	Fourier transform infrared spectroscopy.
WF	Water film.

References

1. Illuzzi, F.; Thewissen, H. Perfluorocompounds emission reduction by the semiconductor industry. *J. Integr. Environ. Sci.* **2010**, *7*, 201–210. [[CrossRef](#)]
2. Chung, J.K.; Lee, K.Y.; Lee, S.G.; Lee, E.M.; Mo, S.H.; Lee, D.K.; Kim, S.G. The development of scrubber for F-gas reduction from electronic industry using pressure swing adsorption method and porous media combustion method. *Clean Technol.* **2017**, *23*, 181–187.
3. Choi, S.-S.; Park, D.-W.; Watanabe, T. Thermal plasma decomposition of fluorinated greenhouse gases. *Nucl. Eng. Technol.* **2012**, *44*, 21–32. [[CrossRef](#)]
4. Han, S.-H.; Park, H.-W.; Kim, T.-H.; Park, D.-W. Large scale treatment of perfluorocompounds using a thermal plasma scrubber. *Clean Technol.* **2011**, *17*, 250–258.
5. Chang, M.B.; Chang, J.-S. Abatement of PFCs from semiconductor manufacturing processes by nonthermal plasma technologies: A critical review. *Ind. Eng. Chem. Res.* **2006**, *45*, 4101–4109. [[CrossRef](#)]
6. Choi, S.; Hong, S.H.; Lee, H.S.; Watanabe, T. A comparative study of air and nitrogen thermal plasmas for PFCs decomposition. *Chem. Eng. J.* **2012**, *185*, 193–200. [[CrossRef](#)]
7. Kuroki, T.; Tanaka, S.; Okubo, M.; Yamamoto, T. CF₄ decomposition using low-pressure pulse-modulated radio frequency plasma. *JSME Int. J. Ser. B Fluids Therm. Eng.* **2005**, *48*, 440–447. [[CrossRef](#)]
8. Chen, S.-H.; Živný, O.; Mašláni, A.; Chau, S.-W. Abatement of fluorinated compounds in thermal plasma flow. *J. Fluor. Chem.* **2019**, *217*, 41–49. [[CrossRef](#)]
9. Hong, Y.C.; Kim, H.S.; Uhm, H.S. Reduction of perfluorocompound emissions by microwave plasma-torch. *Thin Solid Films* **2003**, *435*, 329–334. [[CrossRef](#)]
10. Kiehlbauch, M.W.; Graves, D.B. Temperature resolved modeling of plasma abatement of perfluorinated compounds. *J. Appl. Phys.* **2001**, *89*, 2047–2057. [[CrossRef](#)]
11. Li, Y.D.; Paganessi, J.E.; Rufin, D. Emission reduction of perfluorocompounds in semiconductor manufacturers via capture and recycle. *Green Eng.* **2000**, *6*, 62–75.
12. Mangindaan, D.; Kuo, C.C.; Lin, S.Y.; Wang, M.J. The diffusion-reaction model on the wettability gradient created by SF₆ plasma. *Plasma Process. Polym.* **2012**, *9*, 808–819. [[CrossRef](#)]
13. Wang, C.; Lai, P.-C.; Syu, S.H.; Leu, J. Effects of CF₄ plasma treatment on the moisture uptake, diffusion, and WVTR of poly (ethylene terephthalate) flexible films. *Surf. Coat. Technol.* **2011**, *206*, 318–324. [[CrossRef](#)]
14. Park, H.-W.; Cha, W.B.; Uhm, S. Highly efficient thermal plasma scrubber technology for the treatment of perfluorocompounds (PFCs). *Appl. Chem. Eng.* **2018**, *29*, 10–17.
15. Yoon, J.; Kim, Y.; Song, H. Effect of Inlet Shape on Thermal Flow Characteristics for Waste Gas in a Thermal Decomposition Reactor of Scrubber System. *Appl. Chem. Eng.* **2018**, *29*, 510–518.
16. Park, H.-W.; Choi, S.; Park, D.-W. Effect of reaction gases on PFCs treatment using arc plasma process. *Clean Technol.* **2013**, *19*, 113–120. [[CrossRef](#)]
17. Kim, T.-W.; Jo, G.-Y.; Lee, S.-M.; Lee, K.-H.; Jin, Y.-J.; Son, B.-K. A Study on Direct Current Arc Plasma Torch Design with Preserve Nozzle for Perfluorinated Compounds (PFCs) Decomposition in Cement Kiln. *Appl. Sci. Conver. Technol.* **2021**, *30*, 137–140. [[CrossRef](#)]
18. Lim, M.S.; Kim, S.C.; Chun, Y.N. Decomposition of PFC gas using a water jet plasma. *J. Mech. Sci. Technol.* **2011**, *25*, 1845–1851. [[CrossRef](#)]

19. EPA (2023). Inventory of U.S. Greenhouse Gas Emissions and Sinks: 1990–2021. U.S. Environmental Protection Agency, EPA 430-R-23-002. Available online: <https://www.epa.gov/ghgemissions/inventory-us-greenhouse-gas-emissions-and-sinks-1990-2021> (accessed on 13 April 2023).
20. Moon, G.-H.; Kim, J.-Y. Study on treatment characteristics of perfluorinated compounds using a high temperature plasma. *Appl. Chem. Eng.* **2019**, *30*, 108–113.
21. Lee, J.-Y.; Lee, J.-B.; Moon, D.-M.; Souk, J.-H.; Lee, S.-Y.; Kim, J.-S. Evaluation method on destruction and removal efficiency of perfluorocompounds from semiconductor and display manufacturing. *Bull. Korean Chem. Soc.* **2007**, *28*, 1383–1388.
22. Efremov, A.; Lee, J.; Kim, J. On the control of plasma parameters and active species kinetics in $\text{CF}_4 + \text{O}_2 + \text{Ar}$ Gas Mixture by CF_4/O_2 and O_2/Ar Mixing Ratio. *Plasma Chem. Plasma Process.* **2017**, *37*, 1445–1462. [[CrossRef](#)]
23. Ho, P.; Johannes, J.E.; Buss, R.J.; Meeks, E. Modeling the plasma chemistry of C_2F_6 and CHF_3 etching of silicon dioxide, with comparisons to etch rate and diagnostic data. *J. Vac. Sci. Technol. A Vac. Surf. Film.* **2001**, *19*, 2344–2367. [[CrossRef](#)]
24. Chang, M.B.; Yu, S.J. An atmospheric-pressure plasma process for C_2F_6 removal. *Environ. Sci. Technol.* **2001**, *35*, 1587–1592. [[CrossRef](#)]
25. Takaki, K.; Urashima, K.; Chang, J. Scale-up of ferro-electric packed bed reactor for C_2F_6 decomposition. *Thin Solid Films* **2006**, *506*, 414–417. [[CrossRef](#)]
26. Tschuikow-Roux, E. Kinetics of the Thermal Decomposition of C_2F_6 in the Presence of H_2 at $1300^\circ\text{--}1600^\circ\text{K}$. *J. Chem. Phys.* **1965**, *43*, 2251–2256. [[CrossRef](#)]
27. Su, T.; Kevan, L. Ion cyclotron resonance studies of ionic reactions in perfluorocarbons. Excited ions and their deexcitation. *J. Phys. Chem.* **1973**, *77*, 148–154. [[CrossRef](#)]
28. Su, T.; Kevan, L.; Tiernan, T.O. Positive ion–molecule reactions in perfluoropropane. *J. Chem. Phys.* **1971**, *54*, 4871–4880. [[CrossRef](#)]
29. Christophorou, L.G.; Olthoff, J.K. Electron interactions with C_3F_8 . *J. Phys. Chem. Ref. Data* **1998**, *27*, 889–913. [[CrossRef](#)]
30. Bose, D.; Rao, M.; Govindan, T.; Meyyappan, M. Uncertainty and sensitivity analysis of gas-phase chemistry in a CHF_3 plasma. *Plasma Sources Sci. Technol.* **2003**, *12*, 225. [[CrossRef](#)]
31. Ham, Y.-H.; Shutov, D.A.; Kwon, K.-H. Surface characteristics of etched parylene-C films for low-damaged patterning process using inductively-coupled O_2/CHF_3 gas plasma. *Appl. Surf. Sci.* **2013**, *273*, 287–292. [[CrossRef](#)]
32. Kokkoris, G.; Goodyear, A.; Cooke, M.; Gogolides, E. A global model for C_4F_8 plasmas coupling gas phase and wall surface reaction kinetics. *J. Phys. D Appl. Phys.* **2008**, *41*, 195211. [[CrossRef](#)]
33. Kokkoris, G.; Panagiotopoulos, A.; Goodyear, A.; Cooke, M.; Gogolides, E. A global model for SF_6 plasmas coupling reaction kinetics in the gas phase and on the surface of the reactor walls. *J. Phys. D Appl. Phys.* **2009**, *42*, 055209. [[CrossRef](#)]
34. Xiao, H.; Zhang, X.; Hu, X.; Zhu, Q. Experimental and simulation analysis on by-products of treatment of SF_6 using dielectric barrier discharge. *IEEE Trans. Dielectr. Electr. Insul.* **2017**, *24*, 1617–1624. [[CrossRef](#)]
35. Matsugi, A.; Shiina, H.; Takahashi, A.; Tsuchiya, K.; Miyoshi, A. Burning velocities and kinetics of $\text{H}_2/\text{NF}_3/\text{N}_2$, $\text{CH}_4/\text{NF}_3/\text{N}_2$, and $\text{C}_3\text{H}_8/\text{NF}_3/\text{N}_2$ flames. *Combust. Flame* **2014**, *161*, 1425–1431. [[CrossRef](#)]
36. Choi, S. Microwave thermal decomposition of CF_4 using $\text{SiC-Al}_2\text{O}_3$. *J. Environ. Sci. Int.* **2013**, *22*, 1097–1103. [[CrossRef](#)]
37. Akhgarnusch, A.; Hockendorf, R.F.; Beyer, M.K. Thermochemistry of the reaction of SF_6 with gas-phase hydrated electrons: A benchmark for nanocalorimetry. *J. Phys. Chem. A* **2015**, *119*, 9978–9985. [[CrossRef](#)]
38. Liu, X.; Zhang, J.; Zhang, R.; Hou, H.; Chen, S.; Zhang, Y. Photoreduction of nitrogen trifluoride with controlled release of radicals. *J. Chem. Technol. Biotechnol.* **2014**, *89*, 436–447. [[CrossRef](#)]

Disclaimer/Publisher’s Note: The statements, opinions and data contained in all publications are solely those of the individual author(s) and contributor(s) and not of MDPI and/or the editor(s). MDPI and/or the editor(s) disclaim responsibility for any injury to people or property resulting from any ideas, methods, instructions or products referred to in the content.